Magnetopause reconnection impact parameters from multiple spacecraft magnetic field measurements

Deirdre E. Wendel[1] and Patricia H. Reiff[1]

Received 28 July 2009; revised 29 September 2009; accepted 2 October 2009; published 30 October 2009.

[1] We present a novel technique that exploits multiple spacecraft data to determine the impact parameters of the most general form of magnetic reconnection at the magnetopause. The method consists of a superposed epoch of multiple spacecraft magnetometer measurements that yields the instantaneous magnetic spatial gradients near a magnetopause reconnection site. The gradients establish the instantaneous positions of the spacecraft relative to the reconnection site. The analysis is well suited to evaluating the spatial scales of singular field line reconnection, which is characterized by a two-dimensional x-type topology adjacent and perpendicular to a reconnecting singular field line. Application of the method to Cluster data known to lie in the vicinity of a northward IMF reconnection site establishes a field topology consistent with singular field line reconnection and a normal magnetic field component of 20 nT. The corresponding current structure consists of a 130 km sheet possibly embedding a thinner, bifurcated sheet.
Citation: Wendel, D. E., and P. H. Reiff (2009), Magnetopause reconnection impact parameters from multiple spacecraft magnetic field measurements, *Geophys. Res. Lett.*, *36*, L20108, doi:10.1029/2009GL040228.

1. A Northward IMF Reconnection Event

[2] Collisionless magnetic reconnection is a fundamental process that occurs in many natural and artificial plasmas. We look to the Earth's magnetopause as a natural laboratory to provide us with data on the spatial scales of magnetic reconnection. An array of satellites such as the Cluster mission provides a means to capture the instantaneous scales of magnetic reconnection in the magnetopause. In this paper we present a novel and generic technique that exploits Cluster's multiple spacecraft measurements to estimate the instantaneous reconnection magnetic topology, current sheet thickness, and particle diffusion scales.

[3] For purposes of explication, we apply the technique to a long-lived northward Interplanetary Magnetic Field (IMF) reconnection event first observed by the IMAGE spacecraft [*Frey et al.*, 2003]. During this event of 18 March 2002, the Cluster four-satellite suite crossed the magnetopause at a location mapping along field lines to an ionospheric H-alpha emission caused by proton precipitation from reconnection at the magnetopause [*Phan et al.*, 2003; *Frey et al.*, 2003]. From 14:54 to 15:03 UT, Cluster passed from the northern tail lobe through the magnetopause, at 77.8° magnetic latitude and 12.2 MLT, into the magnetosheath, moving primarily along the noon-midnight meridian northward and towards the sun. Using Tsyganenko '89, '96, and '01 model field lines, *Phan et al.* [2003] mapped the Cluster position at about 15:00 UT to the ionospheric proton spot observed at the same time at about 80° latitude and 2:30 MLT (in apex geomagnetic coordinates) by the IMAGE FUV SI-12 instrument. This implies that Cluster was in the vicinity of the reconnection site at the magnetopause at the time the reconnection footprint was observed at the ionosphere by IMAGE.

[4] We examine this event using Cluster's four-point magnetic field measurements to develop a new technique to determine an instantaneous coordinate system centered on the reconnection line, which we will refer to as the x-line. Our goal will be to establish a magnetic topology consistent with the most general form of magnetic reconnection, i.e., singular field line reconnection, and estimate the resulting spatial dimensions. Singular field line reconnection is defined by a field line—the singular line—that threads a nearby hyperbolic "x" topology in a plane perpendicular to the field line and that carries a parallel electric field [*Priest and Forbes*, 2000].

2. Magnetic Field Data: Features Characteristic of Reconnection

[5] During the magnetopause crossing, Cluster 1 observed a series of nulls in the GSE x and z components of the magnetic field (Figure 1a). (The magnetopause lies roughly between the dotted lines.) Though we show the data for Cluster 1, the magnetic field data is very similar between spacecraft. A proper analysis of this data, however, requires a rotation from the GSE system to one aligned with the local magnetopause—and preferably one where only the x component remains on each side of the magnetopause after rotation. Qualitatively, we wish to align ourselves with the current sheet in the magnetopause, so that the new y direction is parallel to the magnetopause current and the x-line. In other words, we are seeking the large-scale coordinate system for anti-parallel reconnection—one in which only a B_x component exists on either side of the magnetopause. We then identify the current sheet crossings as those locations where the new B_x component changes sign. If, within this coordinate system, we can identify a singular field line topology with either an x-type null or an x-type hyperbolic geometry perpendicular to a magnetic field component along the current sheet, then we have established the first step in satisfying the necessary and sufficient conditions for reconnection. The final step is the detection of a parallel electric field along the singular field line.

[6] To establish the best rotation angles, we use a Minimum Variance Analysis (MVA). The MVA requires

[1]Physics and Astronomy Department, Rice University, Houston, Texas, USA.

0094-8276/09/2009GL040228$05.00

at least three magnetic field values—one before, one during, and one after the boundary crossing [*Sonnerup and Scheible*, 1998]. We first rotate the data by different sets of Euler angles, testing each set of rotation angles by the MVA to determine which set is best. The set of input data to the MVA consists of an interval on each side of the magnetopause (the "before" and "after" inputs to the MVA) and the interval of the magnetopause (the "intermediate" input to the MVA). The angles that minimize the variance along the normal to the boundary and maximize it along the boundary in the MVA comprise the best set of rotation angles. We apply the test to all four spacecraft. A rotation of 52° about the GSE y-axis, 20° about the new z axis, and, finally, 10° about the newest x axis gives the best normal in the final z direction and the best alignment of the current sheet with the y direction. (The best rotation angle about the z-axis ranges between about 17° and 30°, depending on the spacecraft. An angle of 20° is the average that works best for all spacecraft.) With these rotation angles, the MVA gives a maximum eigenvalue in the new x direction, an intermediate value in the y direction, and a minimum value in the new z direction, as desired. The angles coincide very closely with the angles that best remove the average B_z and B_y fields on either side of the boundary. To test the stability of the MVA to averaging over varying interval lengths, we apply the MVA to a range of sub-interval sizes in the magnetopause and find the method is stable.

[7] Figure 1b shows the rotated data from Figure 1a. As desired, only the B_x component remains on either side of the magnetopause after rotating the coordinates. We note that all references to the magnetic field henceforth refer to the rotated coordinates, though we will continue to denote them by unprimed variables, B_i. The bottom plot of Figure 1a displays the magnitude of the magnetic field. Though there is a minimum of about 30 nT in the magnitude, there are no true nulls (i.e., $\mathbf{B} \equiv 0$). As Figure 1b demonstrates, however, there are nulls in the B_x-B_z components. These are the components we expect to reconnect at Cluster's location near the noon-midnight meridian. (As we will discuss, there is also a B_y component that exists only within the magnetopause.) The rotated fields show that they are very nearly antiparallel on either side of the magnetopause (a rotation angle of about 175°), with a positive B_y associated with the current sheet crossings throughout the magnetopause. Figure 1 shows that there are multiple current sheet crossings in the magnetopause, identified by those locations where B_x changes sign. At most of these instances there is a normal B_z component that simultaneously changes sign. This pattern suggests Cluster touches or crosses either a single magnetic reconnection site moving with the magnetopause, or multiple current sheets associated with a tearing mode. The B_x-B_z null near 15:00 UT presents the smallest values observed and thus the closest possible approach to a reconnection site. Therefore this study will focus on that interval.

[8] After the rotation, B_y vanishes on both sides of the magnetopause. However, a purely positive B_y manifests itself exclusively inside the magnetopause. Because the local B_y does not change sign when B_z changes sign through the x-line, it is not quadrupolar. However, it is consistent with a singular field line. Thus we have established a singular field line topology within the magnetopause-aligned coordinate system. This most general reconnection topology is locally two-dimensional and invariant along the y direction. We will show in a subsequent paper that we can attribute this singular field line component of the magnetic field along the current sheet to IMF draping and magnetospheric convection—though it is also consistent in principle with separator reconnection.

[9] Our goal is to derive a superposed epoch coordinate system centered on the x-line. A two-dimensional treatment of the reconnection line requires the spatial derivatives $\partial B_x/\partial z$, $\partial B_z/\partial x$, $\partial B_x/\partial x$ and $\partial B_z/\partial z$ at the x-line. Because we base the derivation solely on the magnetic field data, pressure or density gradients play no role in the interpretation of the resulting topology. We create the superposed epoch in three steps: we first identify the location of the x-line by the minima in B_x-B_z; we then compute the distance of the spacecraft from the x-line by using the linear gradients of **B** and inverting the corresponding Taylor expansion; finally, we place the spacecraft in a coordinate system with the x-line at the center, using the distances we calculate in the second step.

[10] A superposed epoch based on the minima of $\sqrt{B_x^2 + B_z^2}$ yields an estimate of the field gradients near the x-line. It is possible to derive robust estimates of these gradients from a superposed epoch of the spacecraft magnetic fields at only those points where each spacecraft passes closest to the B_x-B_z minimum. Though limited to linear fields close to the minima, these estimates do not suffer from the errors of the curlometer method [*Chanteur and Harvey*, 1997; *Dunlop et al.*, 2002]. We first filter the magnetic field data using a zero-phase forward and reverse digital filter, which produces zero phase distortion. We filter in the frequency range 0.1 to 1.3 Hz, where waves obscure the lower frequency trends of the x-line. Because these slow trends represent the x-line crossing, their slopes give the gradients near the x-line. All spacecraft that measure a value of $\sqrt{B_x^2 + B_z^2}$ less than 7 nT are placed at (0,0) in the relative coordinate system, assuming that those spacecraft are essentially at the location of the x-line. (We choose 7 nT, because it is the smallest value for which we retain enough values from which to derive significant fits.) The other three spacecraft fall into place around the x-line, based on their instantaneous location relative to the spacecraft that measures the minimum $\sqrt{B_x^2 + B_z^2}$. The values used for the linear fit include data only from these other three spacecraft; the spacecraft observing the minimum value is excluded from the fit. Each one of the spacecraft takes its turn in being closest to the x-line. The pattern that evolves reveals the instantaneous large-scale slope of $B_x(z)$ and of $B_z(x)$ from a best linear fit. (The points are clustered at discrete values of z (in Figure 2a) and x (in Figure 2b), as a result of the nearly fixed spacing of the spacecraft. Thus, when spacecraft 2 measures minimum $\sqrt{B_x^2 + B_z^2}$ and is thus assigned to $x = z = 0$, for example, spacecraft 3 is always found at $(x, z) = (-18.4, -64.8)$, spacecraft 4 at (25, 69.5), and spacecraft 1 at (−44, 69.8).) The fits shown in Figures 2a and 2b as solid curves give the slopes $\partial B_x/\partial z \sim -0.56$ nT/km ± 0.04 nT/km and $\partial B_z/\partial x \sim -0.11$ nT/km ± 0.04 nT/km, where the error bars are determined from the variance in the data. The R^2 goodness of fit for $\partial B_x/\partial z$ is ∼0.92, and for $\partial B_z/\partial x$ it is ∼0.5. Note that this method gives an instantaneous gradient derived without any assumptions about the

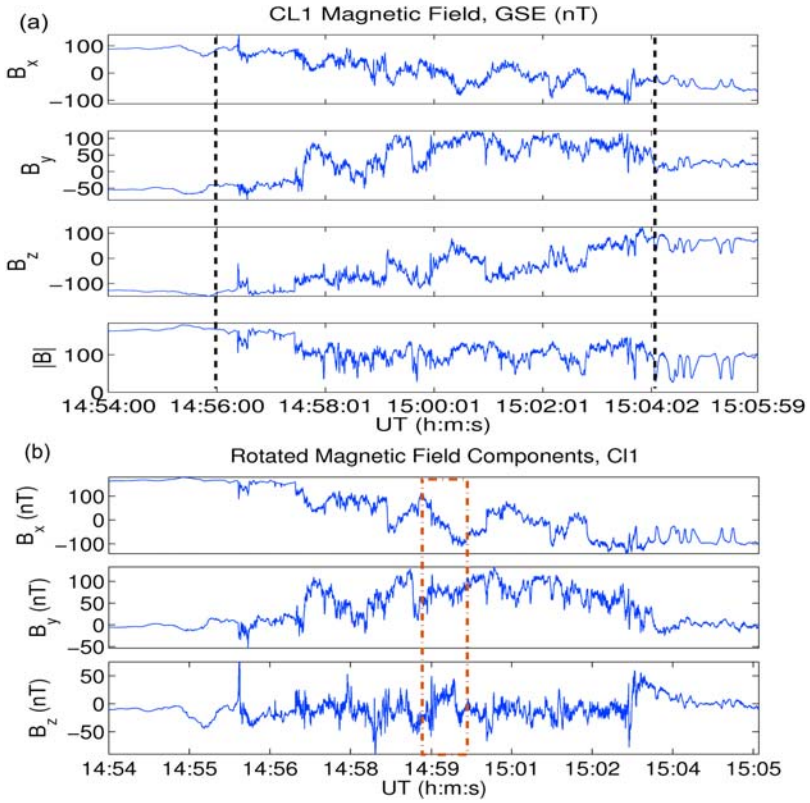

Figure 1. (a) Cluster-1 GSE magnetic field data in the magnetopause. The top three plots show the x, y, and z components, and the bottom plot the total magnitude. (b) Cluster-1 magnetic field data in a boundary normal coordinate system. The data have been rotated into a current sheet-aligned coordinate system.

motion of the x-line relative to the spacecraft. Because there is some low frequency curvature to B_z even after filtering, $B_z(x)$ has some small nonlinearity away from $x = 0$. This nonlinearity will have a small impact on the accuracy of x-line position estimations from data at these x distances.

[11] Our goal is to find the distances of the spacecraft from the x-line at all times near the x-line crossing, and not just at the times when one spacecraft crosses $\sqrt{B_x^2 + B_z^2} <$ 7 nT. To do so, we equate the measured magnetic field values near the x-line with a Taylor expansion for the difference between the measured magnetic field at the known location of the spacecraft and the null in $\sqrt{B_x^2 + B_z^2}$ expected at the x-line (equation (2)). The expansion is statistically linear over the 50 s time window about the x-line crossing (between dashed lines in Figure 1b). At each of the measurement times during this 50 s interval, we place the position and magnetic field values of the spacecraft with the smallest value of $\sqrt{B_x^2 + B_z^2}$ in the Taylor expansion. The positions of the spacecraft (x, z), the magnetic field measurements (B_x and B_z), and the magnetic spatial gradients are known. We then invert the resulting equations for the unknown positions of the x-line, i.e., x_{xl} and z_{xl}, relative to the defining spacecraft:

$$B_x = \left(\frac{\partial B_x}{\partial x}\right)|_{xl}(x - x_l) + \left(\frac{\partial B_x}{\partial z}\right)|_{xl}(z - z_l)$$
$$B_z = \left(\frac{\partial B_z}{\partial x}\right)|_{xl}(x - x_l) + \left(\frac{\partial B_z}{\partial z}\right)|_{xl}(z - z_l) \qquad (1)$$

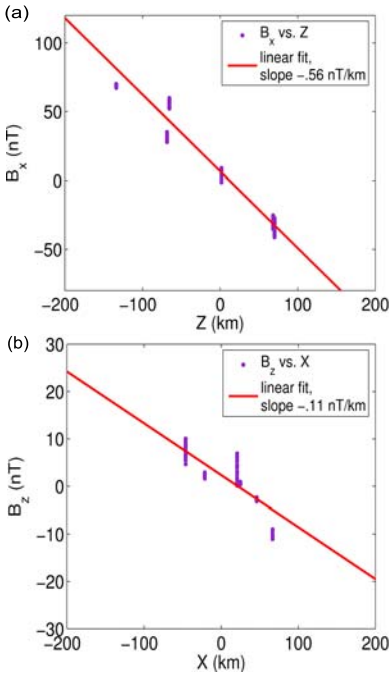

Figure 2. The magnetic field (a) B_x(z) and (b) B_z(x) near the x-line at (0,0). Any spacecraft detecting $(B_x^2 + B_z^2)^{1/2} <$ 7 nT is placed at (0,0). The position values appear discretized because of the fixed spacing of the spacecraft.

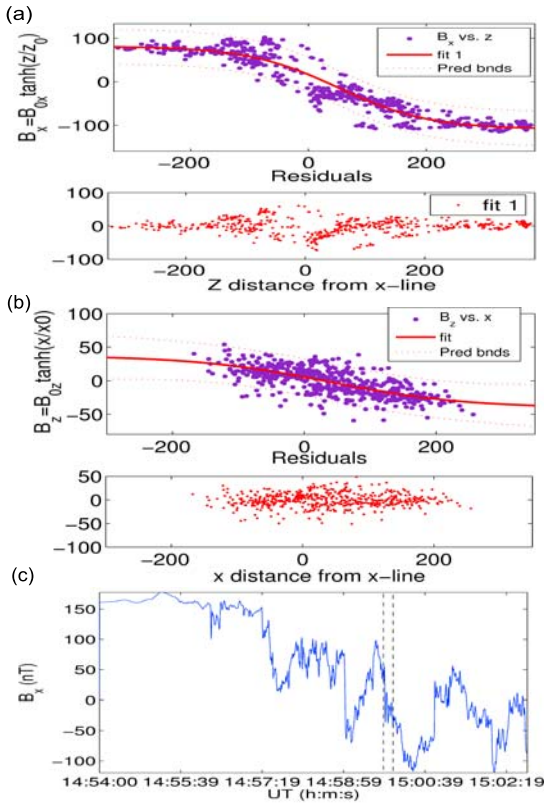

Figure 3. A map of (a) B_x as a function of z and (b) B_z as a function of x at all measurements in a 50 s interval around 15:00 UT. (c) The interval between dotted lines shows a flattened B_x (here from Cluster 1) characteristic of current sheet bifurcation.

The result is an x-line position as a function of time during a 50 s interval during the x-line crossing. Once we have defined the position of the x-line, we make this position the center of the coordinate system and place the spacecraft relative to it.

[12] The curves in Figures 3a and 3b show the tanh functions that are the best fits to the data, namely,

$$B_x(z) = B_{0x}\tanh(z/z_0)$$
$$B_z(x) = B_{0z}\tanh(x/x_0). \quad (2)$$

The use of the tanh function is justified by the roughly linear nature of the magnetic field time series data in this region, and by the general shape of the B_x and B_z data presented in the superposed epoch graphs. The dotted prediction bound curves signify the likelihood a new observation lies within the bounds at the 95% confidence level. The value of the adjusted R-square statistic for the fit to B_x is 0.9, meaning that the fit explains 90% of the variance of the data, assuming the error is random and Gaussian. For the fit to B_z, R^2 is 0.5. The fluctuations have a larger impact on the smaller trend of B_z.

[13] The propagation of errors in the inversion for the x-line position arises from the errors in the spacecraft relative positions, in the linear assumption, and in the estimates of the magnetic spatial gradients. The farther from the minimum in B_x and B_z, the larger the error. At the farthest edges of the curves in Figures 3a and 3b, the error in the x position of the x-line is at most about 80 km, and in the z position, about 60 km. However, closer to the central, linear region of the curves, the error in the x position varies between 3 and 16 km, while that of the z position between 3 and 8 km.

[14] There is evidence for an embedded thin, bifurcated current sheet, in the deviations from the tanh fit. There is a signature of bifurcation—a flattening of the tanh curve near the origin—in Figure 3a. This is difficult to resolve from Figure 3a, but is more obvious in the raw time series signature, as shown in Figure 3c. The area between dotted lines is a region of flattened B_x (here from Cluster 1) that characterizes current sheet bifurcation. This feature can be seen in the magnetic field data from all four spacecraft. Interestingly, the residuals of the tanh fits are largest in a region near the origin. This is not caused by larger position errors near the origin, as in fact these are smallest at the origin. Therefore, the larger residuals are caused by a poorer fit to the tanh function near the origin, not by propagation of errors. This is consistent with the interval where an embedded thin, bifurcated current sheet would show itself.

[15] The fit to B_x gives an instantaneous current sheet thickness, since we have derived it in a coordinate system centered on the reconnection line, with the x-line and the current sheet oriented in the out-of-plane y direction. If the operational definition of the current sheet thickness is full-width at half-maximum, from Figure 3a the current sheet thickness is approximately 130 km. The fit to the $B_z(x)$ data in Figure 3b yields a significant asymptotic reconnection B_{0z} of approximately 20 nT. This normal component would produce a reconnection electric field of roughly $E_y = -4$ mV/m and a polar cap potential drop of about 26 kV, given a reconnection width of 1 R_E and the perpendicular solar wind speed of roughly −200 km/s (measured by the ACE spacecraft) in the rotated coordinate system.

[16] We advance the analysis by placing data in two dimensions surrounding the x-line at the spacecraft positions defined from the inversion of equation (2). In Figure 4, the hyperbolic solid curves are sample field lines chosen to lie at $x = x_0$ and $z = z_0$, one "scale height" away from the separatrix. They are derived by integrating the differential equations $dz/dx = B_z/B_x$, where B_x and B_z are given by the tanh functions. We use the superposed epoch technique to place all four spacecraft about the singular field line. Figure 4a portrays the B_y values by color. The sun and lower latitudes are toward the left. It is clear that B_y maximizes near the x-line, a geometry consistent with a singular field line, as discussed in the introduction. Figure 4b depicts the individual 0.25 s B_x-B_z vectors, revealing a statistically good fit to the hyperbolic model, as expected, in terms of both field magnitude and direction.

3. Summary

[17] This study introduces a set of tools for the vetting of *in situ* reconnection 'sightings' in spacecraft data. The technique exploits multiple spacecraft data to remove the motion of the reconnection site and establish instantaneous spatial scales of the reconnection region. With the Cluster magnetic field data from a northward IMF reconnection event, we find a cusp magnetic field consistent with singular

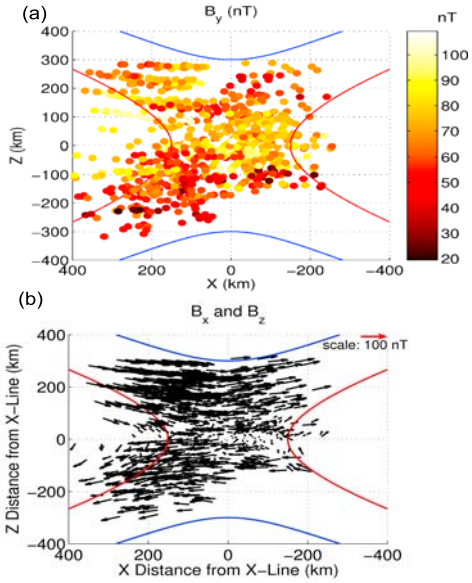

Figure 4. (a) Superposed epoch of B_y and (b) superposed epoch of B_x-B_z. The magnitude of B_y is represented by color, and that of B_x-B_z by the length of the arrows.

field line reconnection. With this topology, a singular field line threads nearby perpendicular magnetic fields that vanish in an x-type geometry. We find a 130 km thick current sheet possibly embedding a thinner, bifurcated current sheet.

[18] Proof of reconnection requires an electric field parallel to the singular field line. Cluster, measuring only two components of the electric field, lacks the necessary data to find the parallel electric field in general. However, one can, in principle, determine a nonideal MHD electric field that deviates from $-\mathbf{v} \times \mathbf{B}$ and a hyperbolic particle flow pattern in the superposed epoch coordinate system as a proxy for a parallel electric field. One can compare the two components of the electric field measured by each spacecraft in its de-spun inertial coordinates to the same two components of the $-\mathbf{v} \times \mathbf{B}$ drift electric field determined from particle moments and the magnetic field. Discrepancies between the measured components of $\mathbf{E}$ and the corresponding components of $-\mathbf{v} \times \mathbf{B}$ after a careful error analysis signify a nonideal electric field. We intend to show in a subsequent paper that the Cluster electric field and particle flow data for this event satisfy the criteria for a parallel electric field.

[19] With the instantaneous coordinate system and the parallel electric field established, one can place particle moments, such as velocities, pressures, and temperatures, as well as magnetic and electric field measurements, around the singular field line for an estimate of their instantaneous spatial distribution. Sufficiently accurate ion and electron moments and electric field measurements within this coordinate system delineate ion and electron diffusion regions.

[20] **Acknowledgments.** We acknowledge the ACE team and the Cluster FGM team for data used in this study. We are grateful to Melvyn Goldstein and Elizabeth Lucek for their feedback on this article. This research has been supported in part by NASA under grants NAG5-13219 and NNX-06AC60G.

References

Chanteur, G., and C. C. Harvey (1997), Spatial interpolation for four spacecraft: Application to magnetic gradients, in *Analysis Methods for Multi-Spacecraft Data*, edited by G. Paschmann and P. W. Daley, pp. 371–393, Eur. Space Agency, Noordwijk, Netherlands.

Dunlop, M. W., A. Balogh, K.-H. Glassmeier, and P. Robert (2002), Four-point Cluster application of magnetic field analysis tools: The Curlometer, *J. Geophys. Res.*, *107*(A11), 1384, doi:10.1029/2001JA005088.

Frey, H. U., T. D. Phan, S. A. Fuselier, and S. B. Mende (2003), Continuous magnetic reconnection at Earth's magnetopause, *Nature*, *426*, 533–537, doi:10.1038/nature02084.

Phan, T. D., et al. (2003), Simultaneous Cluster and IMAGE observations of cusp reconnection and auroral proton spot for northward IMF, *Geophys. Res. Lett.*, *30*(10), 1509, doi:10.1029/2003GL016885.

Priest, E. R., and T. G. Forbes (2000), *Magnetic Reconnection: MHD Theory and Applications*, Cambridge Univ. Press, Cambridge, U. K.

Sonnerup, B. U. Ö., and M. Scheible (1998), Minimum and maximum variance analysis, in *Analysis Methods for Multi-Spacecraft Data*, edited by G. Paschmann and P. W. Daley, pp. 185–220, Eur. Space Agency, Noordwijk, Netherlands.

P. H. Reiff and D. E. Wendel, Physics and Astronomy Department, Rice University, P.O. Box 1892, Houston, TX 77005, USA. (dew52@columbia.edu)